COBEM 2023 27TH INTERNATIONAL CONGRESS OF MECHANICAL ENGENEERING

ABCM Brazilian Society of Mechanical Sciences and Engineering
27th ABCM International Congress of Mechanical Engineering
December 04-08, 2023, Florianópolis-SC, Brazil

COB-2023-1169
ANALYSIS AND VALIDATION OF WAVE ABSORPTION STRATEGIES FOR CFD SIMULATION USING OPENFOAM

Samuel Nobre Chaves Gonçalves
Ernane Silva
CTJ – Technical Centre of Joinville, UFSC – Federal University of Santa Catarina, Joinville/SC, Brazil
samuel.goncalves@teg.ufsc.br
ernane.silva@teg.ufsc.br

Pedro Cardozo de Mello
Escola Politécnica, Universidade de São Paulo, São Paulo, SP, Brasil
pcmello@usp.br

Thiago Pontin Tancredi
Filipe Dutra da Silva
André Luís Condino Fujarra
CTJ – Technical Centre of Joinville, UFSC – Federal University of Santa Catarina, Joinville/SC, Brazil
thiago.tancredi@ufsc.br
filipe.dutra@ufsc.br
andre.fujarra@ufsc.br

Abstract. *The fatigue evaluation of floating platform moorings has been increasingly necessary due to the early failure of several installations around the world in the last years. The phenomena responsible for this problem are classified as fluid-structural interactions, and one of them is wave-induced motion. Motions in platforms can raise the insecurity of its operation, but even in situations where the platform operations are not affected by wave action, they put in proof the life in fatigue of the mooring systems, making them vulnerable to failures earlier than expected, as also needing more periodic maintenance and, consequently, increasing the cost of the whole platform operation. In the final design phases, the performance of the combination of these parameters can be evaluated through Computational Fluid Dynamics (CFD) simulations of wave-induced platform motions for different frequencies, where the motion amplitudes can be evaluated based on the designed mooring system and the Response Amplitude Operator (RAO) curve can be obtained, which describes the platform's seakeeping based on the main dimensions and mass. Previous studies by the authors using the open source CFD software OpenFOAM involving floating body dynamics with simple geometries served as an initial approach to the study of wave energy converters but also contributes to the study of floating platforms. The wave generation model utilized in the previous study, despite low discrepancies in relation to the experimental data, was considered validated due to its low computational cost and the fact that the comparison of the numerical versus experimental data in the reference study also presented discrepancies in the same magnitude order. In order to advance the study within the scope of improving the correlation between numerically simulated and experimentally generated waves, this paper describes the implementation and evaluation of different strategies for passive wave absorption which include porous regions and physical beaches together with the native active absorption of the olaFlow extension, also responsible for the wave generation, in addition to self-authored experimental results to validate the numerical model. The solution that gave the best results for a selected wave in relation to its input parameters was the beach-shaped porous region. With the optimized absorption case, three waves were simulated which had their values compared with the experimental data, showing an excellent correlation.*

Keywords: *Wave Absorption, CFD Simulations, OpenFOAM, Floating Platforms, Experimental Validation*

1. INTRODUCTION

Floating platforms, whether used for oil and gas exploration, offshore wind farms, or other marine activities, are subject to a wide range of dynamic interactions, including waves, winds, and currents, which cannot be perfectly predicted due to their natural randomness. Furthermore, understanding the response of the platform to all these possible loads is essential to ensure operational safety, optimal performance, and structural integrity of the mooring systems during the life cycle of the platform (Sarpkaya, 2010). According to Faltinsen (1990), considering all environmental interactions with the platform, wave-induced motions are among the most impactful, as they can make operations unfeasible and put the entire

structure at risk. Even if the mooring lines successfully damp the movement so that the operations are unaffected, they can get overloaded or doomed to fatigue failure if the design does not predict the platform behaviour under wave action, which was pointed by Xue *et al.* (2018) as one of the main failure modes of a floating platform. The platform motion analysis commonly performed for wave-structure interaction is through the Response Amplitude Operator (RAO), which relates wave and body motion amplitudes for a wide range of frequencies. RAO evaluation gives possible insight into the dynamic behavior of floating platforms in terms of motion characteristics, potential risks evaluation, optimization of structural configurations and development of effective control strategies.

Given the fact that the RAO curve depends on the geometry and mass properties of the platform, it is necessary to submit the body to waves of different frequencies to generate each point of the RAO curve. The traditional method, recently applied in Kamarlouei *et al.* (2020) and Sarmiento *et al.* (2019), is done experimentally in wave tanks by subjecting a reduced scale model to waves; however, due to the high costs necessary to perform these experiments, the numerical approach using Computational Fluid Dynamics (CFD) comes in handy. Even having lower costs and greater flexibility to try different scenarios, the CFD approach brings other concerns such as assumptions on the mathematical models, precision of the numerical methods and numerical errors due to discretization which can all lead to unreal results (Versteeg and Malalasekera, 2007). These uncertainties make it necessary to numerically validate the models by comparing them with experimental results to improve their reliability, as in Shiohara *et al.* (2020) and Ahn and Shin (2020).

Using OpenFOAM, the authors previously studied floating body dynamics for initial studies of wave energy converters with low computational cost (Silva *et al.*, 2021), which are also applicable to floating platform motions. In that study, a reference (Windt *et al.*, 2020) was used to validate the wave generation, and it had errors due to wave reflection at the end of the numerical domain, but since the errors were in the same magnitude order as the reference, the model was validated. That being said, to improve the numerical wave generation initially studied by the authors for the purposes described, this study will focus on passive strategies evaluation for minimizing wave reflection on a Numerical Wave Tank (NWT) simulated in OpenFOAM and comparing the performance of the best strategy with self-authored experimental data for different waves. Improvements both in the quality of the generated waves and the validation method will grant more reliability in future simulations, where platforms will be subjected to waves to construct their RAO curves.

2. EXPERIMENTAL DATA

An experimental setup to execute regular waves to validate the NWT was executed in the wave basin of the Numerical Offshore Tank at the University of São Paulo (USP). The Hydrodynamic Calibrator (CH-TPN) is a wave basin specialized in seakeeping tests for offshore engineering. This facility is a square-shaped tank with 14 meters of sides and 4.1 meters deep and is equipped with 152 wave generating/absorbing units. Therefore, it is able to generate waves in any direction, and also mitigate the wave reflection and standing wave formation, emulating a wave basin without borders. A view of the wave basin is presented in Fig. 1.

For wave measurements inside the wave basin, a set of capacitive wave probes was used. A thin coated vertical stretched wire serves as a linear capacitor proportional to the wire length immersed in the water. An electronic circuit transforms the capacitance in voltage to an acquisition data system (ADS), which records it as the elevation of water. Detailed information on the wave basin and the capacitive wave probe can be found in De Mello (2012).

A set of six wave probes (WP01 to WP06) were assigned to the center line of the tank to measure wave propagation during the experiments for several locations. Figure 2 illustrates the assembly of the wave probes. Among others, three monochromatic (regular) waves were calibrated, in period and height, to execute in the wave basin and recorded by the wave probes.

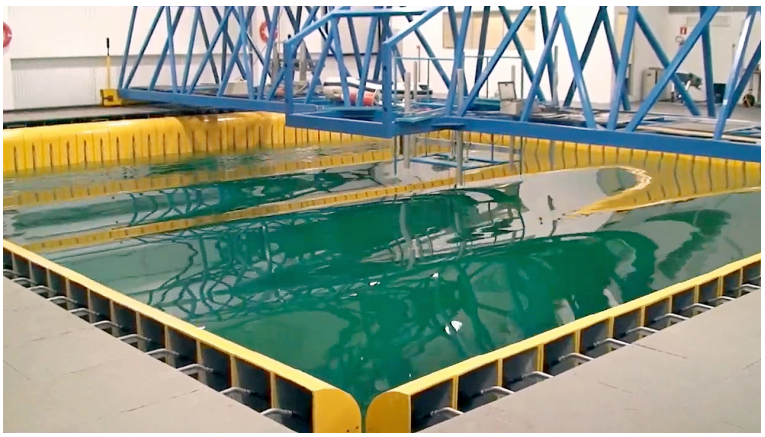

Figure 1. Monochromatic wave in CH-TPN at USP.

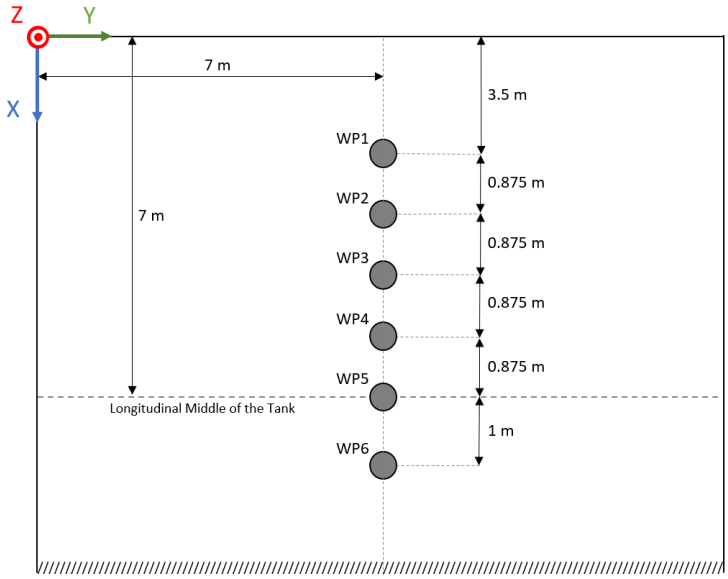

Figure 2. Positions of the wave probes in the tank.

3. NUMERICAL MODEL

3.1 Governing equations

The extension olaFlow was used, which contains wave generation solvers developed in the OpenFOAM framework as a continuation of Higuera (2015) work. The olaFlow can three-dimensionally solve the Volume-Averaged RANS equations (VARANS) for multiphase incompressible turbulent flows using a volume of fluid (VoF) method to distinguish, in this case, water from air volumes. According to Berberovic *et al.* (2009), each phase of an i-th fluid is described, for each cell, by the volume occupation fraction α_i. The main equations considered are the mass and momentum transfer equations, respectively, Eqs. 1 and 2.

$$\nabla \cdot \mathbf{U} = 0 \tag{1}$$

$$\frac{\partial(\rho \mathbf{U})}{\partial t} + \nabla \cdot (\rho \mathbf{U}\mathbf{U}) = -\nabla P + \nabla \cdot (v \nabla \mathbf{U}) + \rho \mathbf{f}_b \tag{2}$$

where ρ is the density, P is the pressure and $\mathbf{U}$ is the velocity field valid for both fluids, v is the molecular viscosity and $\mathbf{f}_b$ is a generic external force.

The fraction volume transport equations for each fluid phase, Eqs. 3 and 4, are simultaneously solved, where α is the volume fraction, having the value 1 for water and 0 for air. The intermediate values of α are undesirable, but can indicate cells on the free surface.

$$\frac{\partial \alpha}{\partial t} + \nabla \cdot (\alpha \mathbf{U}_{water}) = 0 \tag{3}$$

$$\frac{\partial (1-\alpha)}{\partial t} + \nabla \cdot [(1-\alpha)\mathbf{U}_{air}] = 0 \tag{4}$$

$$\frac{\partial \alpha}{\partial t} + \nabla \cdot (\mathbf{U}\alpha) + \nabla \cdot [\mathbf{U}_r \alpha (1-\alpha)] = 0 \tag{5}$$

$$\mathbf{U}_r = \mathbf{U}_{water} - \mathbf{U}_{air} \tag{6}$$

Equations 3 and 4 can be rearranged in the form of a unified equation (Eq. 5), where $\mathbf{U}r$ is called compression velocity, shown in Eq. 6, which has the role of thinning the free surface and reducing the number of cells with value α between 0 and 1 (Berberovic *et al.*, 2009). For the VoF method, all cell properties have values defined as a function of the α index of each cell as

$$\rho = \alpha \rho_{water} + (1-\alpha)\rho_{air}. \tag{7}$$

The olaFlow solver is based on the native interFoam solver of OpenFOAM, which uses the PIMPLE algorithm for pressure-velocity coupling. Generally, the implemented wave generation of the solver consists of reading the wave parameters such as height, period, and theoretical representation, so the surface elevation and velocity field are refreshed at each time step according to the transport equations previously presented. Since turbulent effects are negligible in flows involving waves, as observed by Windt *et al.* (2020), all the simulations in the present study considered laminar flow.

3.2 Passive wave absorption strategies

For numerical analysis, beaches comprising both flow-perpendicular and beach-shaped porous regions were implemented as strategies to reduce wave reflection at the opposite end of the basin model. The absorption conditions considered in the simulations, inspired by Conde *et al.* (2012), are the following:

- No absorption at the end of the NWT;
- Active olaFlow absorption at the end of the NWT;
- 10° and 20° physical beaches;
- 10° beach-shaped porous region with active absorption at the end of the NWT;
- Flow-perpendicular porous region with lengths of $2L$, L, $L/2$ and $L/4$

where L is the total length of the 10° beach. Porosity indices of 30%, 50%, 70% and 90% were also implemented when considered. Figure 3 illustrates the different solutions implemented in OpenFOAM that were compared with the active absorption condition and a vertical wall without absorption.

Figure 3. The implemented passive wave absorbers.

3.3 Computational domain and simulation details

All cases were simulated with two-dimensional domains considering the boundary conditions shown in Fig. 4, with slight variations depending on the tested absorption condition or geometry at the end of the NWT, for example, the physical beach usage or deactivation of the active wave absorption, where in both cases the boundary condition of non-slip (wall) is assumed, and this condition is also applied to the bottom of the domain. For wave generation, a static boundary method based on Stokes wave theory was used, which reduces computational costs because it does not need to compute the mesh movement. At the top, the *pressureInletOutletVelocity* boundary condition was adopted to represent the patch opened to the atmosphere. For the outflow, this boundary condition establishes a zero-gradient condition or a prescribed velocity for the inflow. The olaFlow active wave absorption boundary condition generates a calculated correction velocity $\mathbf{U}_c$ to cancel the incoming waves. To ensure the two-dimensionality, the front and back patches got empty boundary conditions. Concerning the initial conditions, it is considered the wave tank at rest.

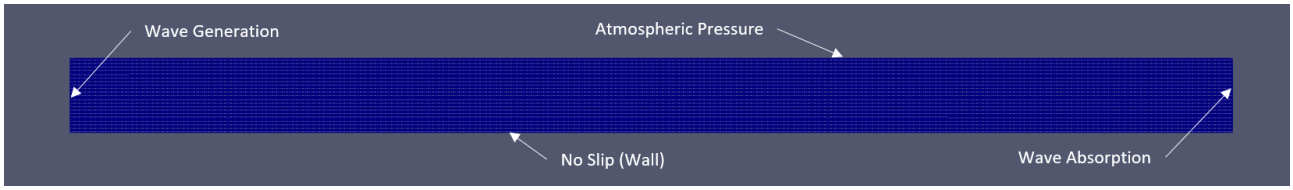

Figure 4. Boundary condition of the meshes.

3.3.1 Wave front simulations

In order to previously evaluate the performance of the wave absorption strategies, a low computational cost base mesh was created with dimensions of 10 m x 0.625 m x 0.425 m of water (length x height x depth). The mesh was generated with 566 cells in the longitudinal direction and 65 cells in the vertical direction, totaling 36790 cells. The mesh for this

case is the same as shown in Fig. 4. It was considered a region of interest of 6.35 m, so in the cases with passive absorbers, they start longitudinally at this point. For the initial comparison, the following methodology was applied for the absorption solutions of 10° physical beach, flow-perpendicular and 10° beach-shaped porous region for a porous index of 50% and vertical wall with and without active absorption of olaFlow.

The previous evaluation of the wave absorbers was made by the 60 s generation of a front of 5 nontransient waves of wave height 0.0238 m of, period 0.714 s, and wavelength 0.92 m which collide into the absorber. A wave probe responsible for tracking the surface elevation is positioned 2 meters away from the wave generator enabling the visual comparative evaluation between absorbers from the free surface profile overtime at the selected position. The cases were simulated in a personal use computer of 8 GB RAM memory and 11th generation i7 2.80 GHz processor, each case took about 30 minutes to run.

3.3.2 Continuous wave generation simulations

For validation purposes, the mesh region of interest used in the continuous-wave generation considered a longitudinal dimension of 14 m, which is the same length at CH-TPN. Due to the variation of the absorber lengths tested in this phase of the study, the final lengths of the meshes for different cases are not the same. To avoid this problem, the mesh construction was entirely parameterized as a function of the wave height and period of the wave in order to keep a ratio of 120 cells per wavelength in the longitudinal direction and 20 cells per wave height in the vertical direction, where deep water theory is respected and applied, for this the water depth considered is half of the wavelength (Dean and Dalrymple, 1991). The cells per wavelength and wave height had values selected according to the ones used in Conde (2019). Figure 5 shows the parametric mesh, where the vertical size determined by the ratio is used to compose the region equivalent to double the wave height. The mesh above and below this refined region has a smooth transition with a cell growth factor of 50 as a way to reduce computational costs in the non-interest regions. Different values for this factor were tested, so the final result was not interfered with by the mesh transition. The total vertical dimension of the mesh is 1.5 times the calculated depth of water for all cases.

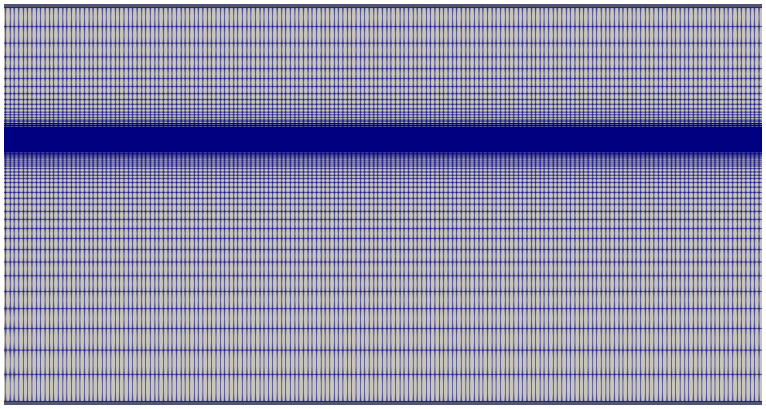

Figure 5. Parametric mesh for continuous wave absorption evaluation.

It was employed the olaFlow solver with the interpolation schemes implemented by Higuera (2015) in the olaFlow tutorial cases and the time-step was selected according the Courant-Friedrichs-Lewy (CFL) condition to guarantee the convergence of the simulations. The CFL condition establishes a relation between the spatial and temporal discretization of the numerical solution of partial differential equations to guarantee stability in solving these problems (De Moura and Kubrusly, 2013). The CFL criterion for the x direction can be seen in Eq. 8, where u is the velocity, t is the time-step and Δx is the logitudinal discretization.

$$C_o = u\frac{\Delta t}{\Delta x} < 1 \tag{8}$$

As you can see from Eq. 8, the higher the spatial discretization, the lower Δt must be to maintain numerical stability on the simulations. It was selected the value of 0.001s for Δt since it was the higher multiple of 10 in which the simulations did not diverge after some tests. In addition it was established an interval of 0.01s for registering the results, leading to an acquisition frequency of 100Hz.

The simulations in this phase of the study consisted of the 100 s generation of a wave with 0.07086 m in height, 3.75 m in length, and a period of 1.55 s (Wave 1). All absorption conditions listed in Section 3.2 were evaluated in this phase of the study. Six wave probes (WP) were implemented at the same longitudinal positions as in continuous wave experiments performed in the CH-TPN at USP; the positioning can be seen in Fig. 2. The last 40 s of the time history results of the six WPs were used for comparison between the absorption strategies in terms of wave height uniformity along the

longitudinal direction and in accordance with the set-up value by processing the signals through Fast Fourier Transform (FFT) analysis.

For the absorption strategy with the best performance, the other two waves were simulated. The parameters of the three waves, as well as the number of cells of each respective parametric mesh, are summarized in Tab. 1.

Table 1. Waves and respective mesh parameters.

Related Parameters	Wave 1	Wave 2	Wave 3
Height [m]	0.07086	0.01298	0.20000
Period [s]	1.55	0.53	1.5
Length [m]	3.75	0.44	3.51
Wave Theory(1)	Stokes II	Stokes II	Stokes III
Number of cells [-]	95800	572880	189696

(1) According to the Lé Méhauté (1976) graph for wave theory coverage.

The cluster from LabCC (Laboratório de Computação Científica) of the Federal University of Santa Catarina (UFSC) was used to simulate these cases, since the computational cost was elevated. Cases were simulated in one 128 GB RAM memory node with an Intel Xeon CPU E5-2640 v420 processor with 20 cores. Wave 1 simulations took half a day each, Wave 3 took approximately 2 days, and Wave 2 simulations took 5 days.

The results were validated through experimental data by comparing the errors related to the set-up values of wave height and period for both numerical and experimental data. It was also possible to evaluate the direct differences between the numerical and experimental results for each WP and calculate the standard deviation for each method.

4. RESULTS AND DISCUSSIONS

4.1 Pre-evaluation of performance

Figure 6 presents the wavefront simulation results for a single WP. The porous beach showed the best performance for wavefront absorption, not presenting major surface elevations after the cease of wave generation, different from the perpendicular porous region, which presented early reflection due to the porous interface acting as a second wall. The porosity effect can be observed by comparing the two 10° beach absorbers where the porosity clearly reduced the peaks of the irregular waves reflected. It was also possible to verify that the olaFlow active wave absorption is not very effective for deep-water conditions given the clear wave reflection observed, similar to the amount reflected by the physical 10° beach.

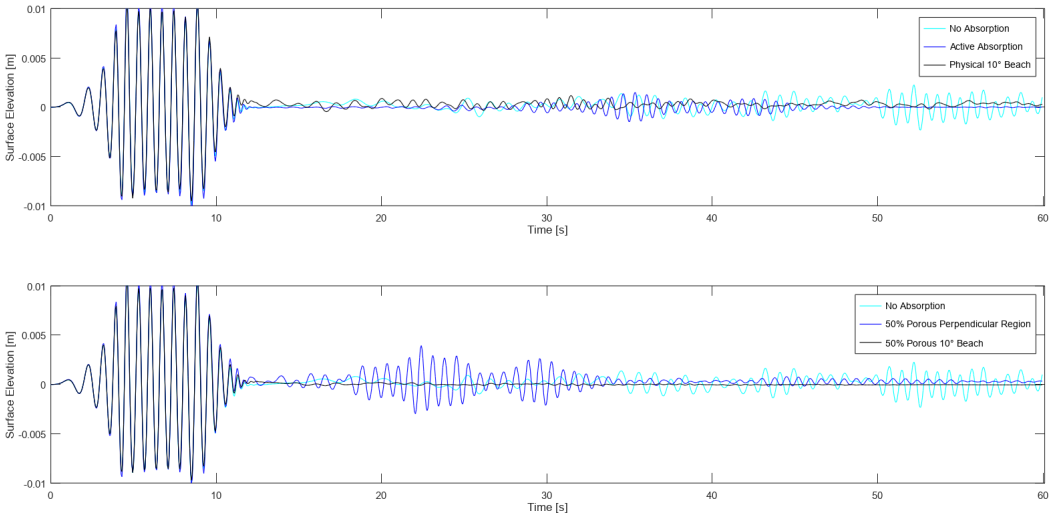

Figure 6. Results of wavefront simulations.

4.2 Comparison of wave absorption strategies for continuous generation

The main results of the absorption strategies performance simulations for Wave 1 are shown in Tab. 2. Active absorption and 20° physical beach had the lowest relative mean errors among all strategies but also had the highest standard deviations, poorly representing Wave 1. For most of the proposed absorption conditions, a standard deviation of the wave

height was obtained that exceeds 14% of the reference wave height, which is equivalent to an almost random surface elevation along the longitudinal direction of the tank. The reason for this high standard deviation is the existence of longitudinal points of strong wave addition and subtraction owing to the steady-state interaction between generated and reflected waves with different phases. A 10-times lower standard deviation was obtained for porous beach absorption in addition to an acceptable value of -5.71% mean relative error, which well represents Wave 1 for steady-state condition.

Table 2. Main results of Wave 1 absorption evaluation for continuous generation.

Wave Height						
Wave Probe	**No Abs.**	**Active Abs.**	**10° Beach**	**20° Beach**	**50% Porous Region**	**50% Porous Beach**
WP1 [m]	0.05447	0.08622	0.06250	0.07421	0.05832	0.06852
WP2 [m]	0.10944	0.05143	0.03629	0.08213	0.08934	0.06770
WP3 [m]	0.07481	0.08822	0.05913	0.05801	0.07162	0.06609
WP4 [m]	0.09473	0.04773	0.04081	0.09259	0.07779	0.06775
WP5 [m]	0.09293	0.08800	0.05461	0.04143	0.08357	0.06431
WP6 [m]	0.09655	0.04688	0.03942	0.09138	0.07904	0.06651
Mean [m]	0.08716	0.06808	0.04879	0.07329	0.07661	0.06681
σ_x [m]	0.01947	0.02132	0.01128	0.02014	0.01074	0.00151
Error$^{(1)}$ [%]	23.00	-3.92	-31.14	3.43	8.12	-5.71

$^{(1)}$ Relative error between mean wave height measures and the reference value 0.07086m.

Combinations for the four porosity indices and the four lengths of the porous region were also simulated for the full porous region strategy, but only resulted in slight variations in the WP values of the porous region 50% shown in Tab. 2. Table 3 shows the comparison between the different porosity indices for the 10° porous beach solution. For higher percentage values of porosity, the mean error and the dispersion decrease. With a porous material of 90%, the simulation resulted in a 3.06% error in the mean wave height and a standard deviation of less than 2% of the wave height. It can be due to the fluid crashing less violently at the interface of a more porous material, which, in addition to the angled geometry of the beach, allows the flow through the porosity to properly dissipate the energy of the wave. Given the great performance of the porous beach and the inability of the other strategies to reliably maintain a constant wave height over the NWT, the chosen absorption solution was the 90% porous 10° beach.

Table 3. Porosity index variation for porous 10° beach strategy.

Porous 10° Beach				
Wave Probe	**Porosity 30%**	**Porosity 50%**	**Porosity 70%**	**Porosity 90%**
WP1 [m]	0.06991	0.06852	0.07011	0.06924
WP2 [m]	0.06677	0.06770	0.06823	0.06898
WP3 [m]	0.06820	0.06609	0.06946	0.06934
WP4 [m]	0.06657	0.06775	0.06786	0.06781
WP5 [m]	0.06671	0.06431	0.06882	0.06948
WP6 [m]	0.06559	0.06651	0.06726	0.06731
Mean [m]	0.06729	0.06681	0.06862	0.06869
σ_x [m]	0.00153	0.00151	0.00105	0.00091
Error$^{(1)}$ [%]	-5.04	-5.71	-3.16	-3.06

$^{(1)}$ Relative error between mean wave height measures and the reference value 0.07086m.

4.3 Model validation

Tables 4, 5 and 6 present the results of the simulations of the three waves with the 70% porous 10° beach absorber and each respective validation experiment. Three columns of errors are presented, in which the first two show the relative errors of the measurements in relation to the set-up value, while the last column present the error between numerical and experimental approach taking the experimental as the reference. .

It was noted that, in relation to the set-up values, the numerical errors were lower than the experimental ones for most of the wave probes for all the waves. In addition, the standard deviation of the wave height measured by the numerical wave probes was lower than that of the experimental measurements.

The Wave 1 simulation had the lowest relative errors, having values lower than 5% for all WPs, which was expected, given that the absorber was selected by tests under the conditions of Wave 1. Wave 3 simulations also presented low relative errors even having a much higher wave height, which reinforces the effectiveness of the absorption solution. On

Table 4. Numerical and experimental results for Wave 1.
Wave height = 0.07086m. Period = 1.55s.

Wave Probe	Experiment		Simulation		Experimental Height Error$^{(1)}$ [%]	Numerical Height Error$^{(1)}$ [%]	Error Between Approaches [%]
	H [m]	T [s]	H [m]	T [s]			
WP1	0.08494	1.76	0.07011	1.49	19.9	-1.1	-17.5
WP2	0.06253	1.78	0.06825	1.49	-11.8	-3.7	9.1
WP3	0.06850	1.78	0.06943	1.49	-3.3	-2.0	1.4
WP4	0.05635	1.79	0.06790	1.49	-20.5	-4.2	20.5
WP5	0.05820	1.73	0.06803	1.49	-17.9	-4.0	16.9
WP6	0.07118	1.74	0.06740	1.49	0.5	-4.9	-5.3

(1) Relative to the wave height of 0.07086m

Table 5. Numerical and experimental results for Wave 2.
Wave height = 0.01298m. Period = 0.53s.

Wave Probe	Experiment		Simulation		Experimental Height Error$^{(1)}$ [%]	Numerical Height Error$^{(1)}$ [%]	Error Between Approaches [%]
	H [m]	T [s]	H [m]	T [s]			
WP1	0.00981	0.53	0.01047	0.51	-24.4	-19.4	6.7
WP2	0.01172	0.53	0.01016	0.51	-9.7	-21.8	-13.3
WP3	0.01122	0.53	0.00992	0.51	-13.6	-23.6	-11.6
WP4	0.01105	0.53	0.00987	0.51	-14.9	-24.0	-10.7
WP5	0.00960	0.53	0.00973	0.51	-26.0	-25.1	1.3
WP6	0.01267	0.53	0.00959	0.51	-2.4	-26.1	-24.3

(1) Relative to the wave height of 0.01298m

Table 6. Numerical and experimental results for Wave 3.
Wave height = 0.2m. Period = 1.5s.

Wave Probe	Experiment		Simulation		Experimental Height Error$^{(1)}$ [%]	Numerical Height Error$^{(1)}$ [%]	Error Between Approaches [%]
	H [m]	T [s]	H [m]	T [s]			
WP1	0.17828	1.51	0.19088	1.45	-10.8	-4.6	7.0
WP2	0.20330	1.51	0.19077	1.45	1.7	-4.6	-6.2
WP3	0.13826	1.48	0.18838	1.45	-30.9	-5.8	36.3
WP4	0.15919	1.48	0.18775	1.45	-20.4	-6.1	17.9
WP5	0.18777	1.50	0.18666	1.45	-6.1	-6.7	-0.6
WP6	0.17812	1.49	0.18476	1.44	-10.9	-7.6	3.7

(1) Relative to the wave height of 0.2m

the other hand, Wave 2 presented, even with values lower than 20%, the highest relative errors, probably due to mesh refinement. Even with the constant value of 20 cells per wave height for the meshes of all waves, it is possible that low wave heights need a lower number of cells with both air and water for the internal surface tracking algorithm of interFoam solver to work best to distinguish water from the air.

More uniformity was reached by the numerical approach, and, for most of the wave probes, the numerical results had more tendency to achieve the desired wave height than the experimental ones. By direct comparison of the numerical and experimental results for each WP through the "Error Between Approaches" columns, all deviations were less than 25%, excluding WP3 from Wave 3, which can be considered an experimental outlier.

5. CONCLUSIONS

The impact of passive wave absorbers on the accuracy of waves in permanent flow was examined through this study. The beach-shaped porous region proved to be the best strategy, since it maintained a uniform wave height along the wave tank with, also, the lowest mean errors. It is inferred that the higher the porosity index, the lower the wave height errors; the most probable reason is that with high porosity indexes, the crash of the waves in the interface becomes smoother to the point of minimizing the wall collision reflection, because the porous region stop behaving as a real wall given that it is highly porous.

The model in Waves 2 and 3 also showed good results for the absorption strategy, having the highest errors for Wave 2, the smaller one. Even with the same parameterized mesh refinement applied for each wave case, Wave 2 seemed to

need extra refinement, which can be evaluated in future studies. With the cross of numerical and experimental results, the numerical model was validated, presenting fewer errors and deviation through the longitudinal dimension of the tank than for Waves 1 and 3. The numerical results for Wave 2 presented errors higher than the experimental ones, but still in an acceptable range.

Future studies will focus on the application of validated wave generation for different contexts such as floating platforms and other geometries RAO generation and evaluation.

6. ACKNOWLEDGEMENTS

The authors thank Doctors Juan Pablo de Lima Costa Salazar and Diogo Nardelli Siebert for their support in using the computational cluster of the LabCC (Laboratório de Computação Científica) of the CTJ-UFSC. The third author also thanks the National Council for Scientific and Technological Development (CNPq), Grant 314057/2021-8.

7. REFERENCES

Ahn, H. and Shin, H., 2020. "Experimental and numerical analysis of a 10 mw floating offshore wind turbine in regular waves". *Energies*, Vol. 13, 2608.

Berberovic, E., Hinsberg, N.P., Jakirlic, S., Roisman, I.V. and Tropea, C., 2009. "Drop impact onto a liquid layer of finite thickness: Dynamics of the cavity evolution". *Physical Review E*, , No. 79, pp. 1–15.

Conde, J.M.P., 2019. "Comparison of different methods for generation and absorption of water waves". *Engenharia Térmica (Thermal Engineering)*, Vol. 18, No. 1, pp. 71–77.

Conde, J.M.P., Capitão, R., Neves, M.G. and Fortes, C.J., 2012. "Comparison of passive wave absorption techniques with evaluation of incident and reflected agitation in a channel (in portuguese)". In *Proceedings of the 2ª Jornada de Engenharia Hidrográfica*. Lisboa.

De Mello, P.C., 2012. *Sistema de automação e controle para tanques oceânicos com múltiplos atuadores*. Ph.D. thesis, São Paulo, Brasil.

De Moura, C.A. and Kubrusly, C.S., 2013. *The Courant-Friedrichs-Lewy (CFL) condition*. Birkhauser, Rio de Janeiro.

Dean, R.G. and Dalrymple, R.A., 1991. *Water wave mechanics for engineers and scientists*. World Scientific, Singapore, 2nd edition.

Faltinsen, O.M., 1990. *Sea Loads on Ships and Offshore Structures*. Cambridge University Press.

Higuera, P., 2015. *Application of computational fluid dynamics to wave action on structures*. Ph.D. thesis, University of Cantabria, Santander, Spain.

Kamarlouei, M., Gaspar, J.F., Calvario, M., Hallak, T.S., Mendes, M.J.C.G. and Thiebaut, F., 2020. "Experimental analysis of wave energy converters concentrically attached on a floating offshore platform". *Renewable Energy*, Vol. 152, pp. 1171–1185.

Lé Méhauté, B., 1976. *Introduction to Hydrodynamics and Water Waves*. Springer-Verlag, New York.

Sarmiento, J., Iturrioz, A., Ayllón, V., Guanche, R. and Losada, I.J., 2019. "Experimental modelling of a multi-use floating platform for wave and wind energy harvesting". *Ocean Engineering*, Vol. 173, pp. 761–773.

Sarpkaya, T., 2010. *Wave Forces On Offshore Structures*. Cambridge University Press.

Shiohara, H., Gonçalves, R.T., Carmo, L.H.S., Schnepf, A., Hirabayashi, S. and Nihei, Y., 2020. "Numerical and experimental comparison of the wave response of a very light floating offshore wind turbine with guy wires". In *Proceedings of the ASME 2020 39th International Conference on Ocean, Offshore and Arctic Engineering OMAE2020*. ASME - The American Society of Mechanical Engineers, Virtual, Online.

Silva, E., Freitas, N.B., Gonçalves, S.N.C., Tancredi, T.P., da Silva, F.D. and Fujarra, A.L.C., 2021. "Cfd simulation of floating-body dynamics for energy conversion using openfoam". In *Proceedings of the 26th International Congress of Mechanical Engineering - COBEM 2021*. ABCM - Brazilian Society of Mechanical Sciences and Engineering, Virtual, Brazil.

Versteeg, H.K. and Malalasekera, W., 2007. *An introduction to computational fluid dynamics: the finite volume method*. Pearson Education, England.

Windt, C., Faedo, N., García-Violini, D., Peña-Sanchez, Y., Davidson, J., Ferri, F. and Ringwood, J.V., 2020. "Validation of a cfd-based numerical wave tank model of the 1/20th scale wavestar wave energy converter". *Fluids*, Vol. 5, No. 3.

Xue, X., Chen, N., Wu, Y., Xiong, Y. and Guo, Y., 2018. "Mooring system fatigue analysis for a semi-submersible". *Ocean Engineering*, Vol. 156, pp. 550–563.

8. RESPONSIBILITY NOTICE

The authors are solely responsible for the printed material included in this paper.